16th Australasian Fluid Mechanics Conference
Crown Plaza, Gold Coast, Australia
2-7 December 2007

The forces on a fish-inspired unsteady hydrofoil

Timothy C. W. Lau and Richard M. Kelso

School of Mechanical Engineering, The University of Adelaide, North Terrace Campus, SA 5005, Australia

Abstract

The flow around an unsteady hydrofoil, undergoing simultaneous heaving and pitching motions which mimic the tail motions of carangiform fish (such as tuna), was investigated using simultaneous particle image velocimetry (PIV) and force measurement. These investigations were performed at Reynolds numbers, based on the foil chord length, in the range of $1500 < Re < 12500$. The Strouhal numbers, based on the foil heave amplitude, were in the range of $0.1 < St_h < 0.95$. Hydrogen bubble visualisation was also performed on the foil at identical St_h, but at $500 < Re < 3500$.

Two force measurements were obtained. Firstly, instantaneous thrust and side forces were obtained by direct strain gauge measurements on the foil, which were then time-averaged. Secondly, time-averaged thrust forces were estimated using a momentum integral around the time-averaged two-dimensional PIV velocity field around the foil. Both force measurements, which show excellent agreement for all foil parameters, indicate that the foil is able to produce very large thrust coefficients, C_t, in excess of 10. These large thrust coefficients typically occur when the non-dimensional foil heave amplitude is large, at conditions where hydrogen bubble visualisation indicates that large leading edge vortices are generated. This suggests that the unsteady foil may be able to use unsteady flow mechanisms to generate large forces.

Introduction

It has often been suggested that, due to evolutionary forces, many aquatic animals are capable of producing large thrust coefficients, or producing thrust very efficiently [9]. This proposition is particularly applicable for the carangiform class of fish (such as tuna and dolphins), which is roughly defined as any aquatic animal that uses the motion of its tail to generate propulsion, due to the fact that carangiform swimmers have been observed to swim continuously for long periods and have been observed to be capable of large accelerations [2, 7, 9].

Traditionally, research in the kinematics of carangiform swimmers has been achieved using unsteady hydrofoils which undergo simultaneous heaving and pitching which mimic the tail motions of carangiform fish. Previous studies on unsteady foils have indicated that such a flow can be strongly characterised by the Strouhal number, St, and to a lesser extent, the maximum foil angle of attack achieved during an entire oscillating cycle, α_{max} [1, 3, 5].

Propulsive efficiencies of over 80% have been recorded [1], occurring roughly at $0.25 < St < 0.35$, which is approximately the same Strouhal number range as observed for fish during steady swimming [6, 8]. Large thrust coefficients, on the other hand, are observed to be generated at higher St, where α_{max} tends to be large [1, 3, 5]. It has been suggested that these large thrust coefficients are developed due to the generation and control of large leading edge vortices [1], possibly indicating that fish use unsteady flow mechanisms during propulsion [2].

This study forms part of a larger investigation of the forces on, and the flow around a heaving and pitching hydrofoil. In particular, we intend to examine a large number of flow cases and foil parameters, using a combination of force measurements and flow visualisation, with the ultimate aim of determining the effect of the foil parameters on the flow, and on the forces developed by the unsteady foil.

Experimental Setup

The motion of a carangiform tail is approximated using a rigid NACA 0026 hydrofoil undergoing simultaneous heaving and pitching motion. The foil has chord length, $c = 50$mm, and a span, $s = 200$mm, giving an aspect ratio of 4.

Two stepper motors, which are phase locked at a flapping frequency f, provide the heaving and pitching motions via a scotch yoke and cam mechanism respectively, as previously described in [4]. The heaving and pitching motions can then be described mathematically as

$$h(t) = h_0 \cdot \cos(2\pi f t - \frac{\pi}{2}) \quad (1)$$

$$\theta(t) \approx \theta_0 \cdot \cos(2\pi f t) \quad (2)$$

where t is time, and the selected heave and pitch amplitudes respectively were $\frac{h_0}{c} = 0.25, 0.5, 0.75$ and $\theta_0 = 0^o, 15^o, 30^o, 45^o$. We define the Strouhal number, based on the heave amplitude as

$$St_h = \frac{2 \cdot h_0 \cdot f}{U_\infty}. \quad (3)$$

where U_∞ is the freestream velocity. Based on the foil dynamics, the relationship between St_h and α_{max} is

$$St_h \approx \frac{\tan(\alpha_{max} + \theta_0)}{\pi} \quad (4)$$

The foil was placed in a recirculating water channel with a working section of 2000mm $\times$ 500mm $\times$ 500mm such that the centre of the foil is aligned to the centre of the water channel working section. This is to ensure that the walls and the free surface of the water channel remain distant to the unsteady foil.

The experiments on the unsteady foil consist of three parts : a) Particle Image Velocimetry (PIV) of the flow in the wake of the foil, b) instantaneous force measurements via strain gauges and c) hydrogen bubble visualisation.

A dual cavity Quantel Brilliant B Twins Nd:YAG pulsed laser, with a fixed pulse rate of 10Hz, was used as the source of illumination for all PIV experiments. The laser pulse is converted into a light sheet approximately 1mm thick using a series of three cylindrical lenses, with focal lengths of 100mm, -50mm and -12.7mm respectively. The resulting light sheet was generated on a plane coincident with the mid-span of the foil. The flow was seeded with hollow glass spheres with a mean diameter of $20\mu m$ and a density of $1030 kg/m^3$. Images of the seeded flow field were captured using a Kodak Megaplus ES 1.0 10bit CCD camera, with a sensor resolution of 1008 $\times$1018 pixels. Two different lenses were used in conjunction with the camera; a Nikkor AF 50mm f/1.4D lens and a Nikkor AF 70-300mm f/4.5-5.6D lens. The size of the field of view was typically set to $\approx 2.5c \times 2.5c$.

For each flow condition, a minimum of 4000 image pairs were collected. Velocity fields were obtained by cross correlating the

image pairs using PIV-View 1.75 (command line interface). A 16×16 pixel interrogation window size was used, with an overlap of 50%. The resultant velocity field consists of 126 (streamwise) ×125 vectors (cross-streamwise) vectors. Velocity outliers were detected using the method suggested by [10]. Typical velocity fields consist of less than 0.1% outliers. All outliers were disabled. A time-averaged velocity field is then obtained by taking the mean of all the valid vectors at each grid point. Due to this time averaging process, the random errors in velocity are estimated to be very low, below 0.5%. No smoothing was performed on the velocity field.

Based on the time-averaged velocity field around the foil, the time-averaged thrust force on the foil can be estimated by performing a momentum balance around the control volume, ABCD, encompassing the foil (as shown in figure 1). If the control volume is sufficiently large such that the x-component of the velocity along the boundaries AB and CD, into the control surface AC is $\approx U_\infty$, and the pressure gradients across the control volume are negligible, then the thrust force based on the PIV velocity field can be approximated by

$$F_{t,piv} \approx \rho_{water} \int_{-b}^{b} U_2(y)\,[U_\infty - U_2(y)]\,dy \tag{5}$$

which can be solved by numerically integrating along the boundary of the PIV-derived time-averaged velocity fields. Equation 5 also assumes that the flows through the sides of the control volume ABCD+ (into the page) and ABCD- (out of the page) are negligible, and the flow is steady. Nonetheless, we expect $F_{t,piv}$ to be a reasonable estimate to the true thrust forces on the foil, due to the fact that the PIV-derived time-averaged velocity fields are steady, encompass a large perimeter around the foil, and are measured along the mid-span of the foil where span-wise flow through the sides of the control volume are expected to be small.

Direct force measurements via strain gauges, performed simultaneously with the PIV experiments, were also conducted on the unsteady foil. Force measurements were made on two orthogonal axes, F_C^* and F_N^* (see figure 1). Each force component was measured using a set of four strain gauges set up in a temperature-compensated Wheatstone bridge. Voltages are then conditioned using an in-house variable gain strain gauge conditioning apparatus, before being measured by a 14-bit data logger (NI-USB 6009) in differential mode. Sampling frequency was fixed at $f_{samp} = 200$Hz, and the typical sampling time was in the order of 10 minutes, leading to approximately 120,000 data samples per force component. The voltage signal was filtered using a digital 4-pole Butterworth filter with a cutoff frequency of 5 Hz. The inertia of the foil was accounted for by subtracting the force measurements performed on the foil when there was no water in the water channel, leading to hydrodynamic force components F_C and F_N. It was then a simple matter to convert the normal and chord-wise foil force components to thrust and side force (in the streamwise and cross-streamwise directions respectively, as shown in figure 1) components, measured using the strain gauge apparatus,

$$F_{t,sg} = -\int_0^T (F_C(t)\cdot\cos\theta(t) + F_N(t)\cdot\sin\theta(t))\cdot dt \tag{6}$$

$$F_{s,sg} = \int_{\frac{T}{4}}^{\frac{3T}{4}} (-F_C(t)\cdot\sin\theta(t) + F_N(t)\cdot\cos\theta(t))\cdot dt \tag{7}$$

where $T = \frac{1}{f}$ is the foil oscillation period.

Finally we define the force coefficient as

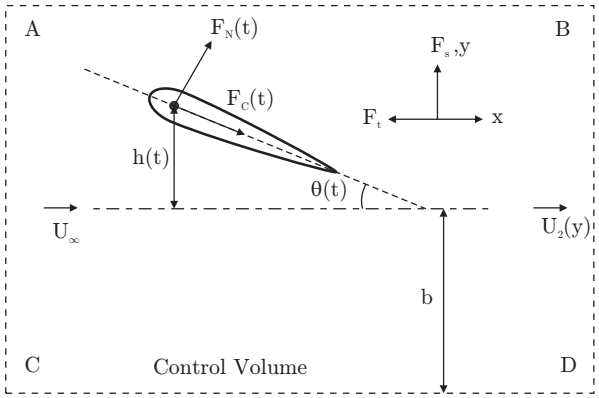

Figure 1: Definition of foil kinematics

$$C = \frac{F}{\frac{1}{2}\rho_{water} U_\infty^2 \cdot c \cdot s} \tag{8}$$

where $s = 1$ and $s = 0.2$ for the PIV and strain gauge thrust measurements respectively. Furthermore, we also define a dimensionless term analogous to the lift:drag ratio, which we name the "productivity", η

$$\eta = \frac{C_t}{C_s} \times 100\% \tag{9}$$

Hydrogen bubble visualisation was also performed on the unsteady foil for a smaller number of foil heave and pitch combinations. The hydrogen bubble wire (50μm tungsten wire) was placed spanning the entire length of the foil on both sides, corresponding to the location of the maximum thickness of the foil. Images of the flow, viewed from the foil spanwise direction, were captured using a Canon EOS 20D digital still camera with a Canon EF 50mm f/1.4 USM lens, at a fixed rate of 8 frames per second.

Results and Discussion

The experiments consisted of force acquisition and PIV measurements across a large number of foil parameters and flow conditions at $1500 < Re_c < 12500$. In this paper, we limit our discussion to two foil heave/pitch combinations, Group I and Group II. In Group I, the foil undergoes moderate heave and pitch amplitudes, $\frac{h_0}{c} = 0.5$ and $\theta_0 = 30^o$, which are representative of the majority of the investigated flow conditions. In Group II, the foil undergoes purely heaving motions, $\frac{h_0}{c} = 0.5$, $\theta_0 = 0^o$, which are representative of heave-dominated flow conditions.

The PIV-derived thrust coefficients and the direct strain gauge thrust and side force coefficients for both groups I and II are shown in figure 2, for a range of Strouhal numbers. The agreement $C_{t,piv}$ and $C_{t,sg}$ for both cases (figures 2a and b) is excellent, indicating that the force measurements are, most likely, accurate.

Interestingly, in all measured cases, we do not observe a sudden drop-off in the thrust coefficient as St_h and α_{max} increases, even beyond the steady-state stall angle (which is estimated to be $\approx 7^\circ - 10^\circ$ at $Re \approx 10000$). In fact, the foil still produces thrust even beyond $\alpha_{max} > 65^o$ (for example, $\alpha_{max} = 66^o$ at $St_h = 0.714$ for Group I) without any sign of stall. Since C_t and C_s show a strong relationship to St_h^2 (which was also noted by [3]), this implies that C_t on the foil can be increased to arbitrarily large values simply by increasing St_h.

Based on these results, it is not surprising that in most flow cases, as represented by group I, the thrust coefficients achieved

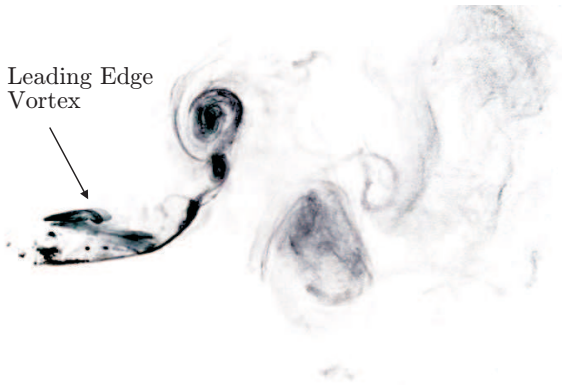

(a) Group I, $\frac{h_0}{c} = 0.5$, $\theta_0 = 30^o$, $St_h = 0.36$, $\alpha_{max} \approx 18.5^o$

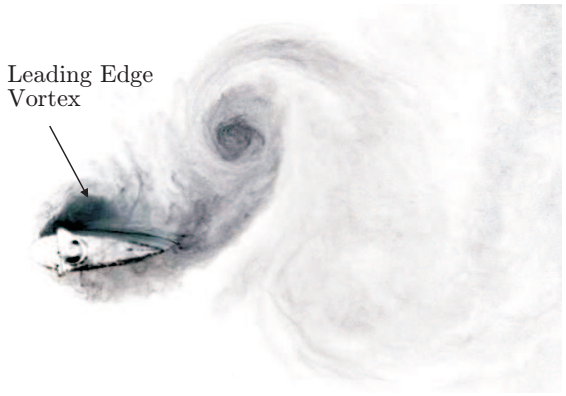

(b) Group II, $\frac{h_0}{c} = 0.5$, $\theta_0 = 0^o$, $St_h = 0.36$, $\alpha_{max} \approx 48.5^o$

Figure 3: Hydrogen bubble visualisation of unsteady foil at its minimum heave position

are moderately high, on order of $C_t \approx 3-4$ at large $St_h \approx 0.7$ (figure 2a). Furthermore, when the heave amplitude is large, the thrust coefficients developed by the foil are very large, exceeding $C_t > 10$ at $St_h \approx 0.7$ (figure 2b), where the maximum angle of attack is also very large ($\alpha_{max} \approx 65^o$).

The results of the hydrogen bubble visualisation indicate that flow around the foil at these high heave amplitudes is dominated by the presence of a strong leading edge vortex (as shown in figure 3b), whereas for most other foil parameters, the leading edge vortex is either small or non-existent (figure 3a). This provides strong evidence that the large C_t values produced by the heave-dominated foil are linked to the generation of a large leading edge vortex, as previously suggested by [1].

The productivities for both groups asymptote to $\eta \approx 40-50\%$ as St_h increases, suggesting that the large values of C_t developed at high St_h coincide with similar increases in C_s. Denoting the mean foil velocity magnitude in the cross streamwise direction as $\overline{|h'(t)|}$, and assuming that the moments on the foil are small, we can estimate the propulsive (Froude) efficiency as

$$\eta_F \approx \frac{F_t \cdot U_\infty}{F_s \cdot \overline{|h'(t)|}} \propto \frac{\eta}{St_h} \tag{10}$$

since it can be shown from equation 1 that $\frac{U_\infty}{\overline{|h'(t)|}} \propto \frac{1}{St_h}$. This implies that the propulsive efficiencies are low at large St_h.

Of additional interest is the x-intercept in figures 2a and 2b, which is the St_h at which the foil is neither producing nett thrust nor drag. This value, $St_0 \approx 0.15-0.3$ in most flow cases, is consistent with the conclusions of our previous study [4]. Thus, if we assume that the forebodies of fish have very low drag, this explains the fact that steadily swimming carangiform fish swim have been observed to swim at $St \approx 0.25$ [6, 8].

Based on these results, we propose two different modes of propulsion :

1. "Cruise Mode" : C_t is low to moderate, and propulsive (Froude) efficiencies are, most likely, relatively high. This occurs at moderate heave and pitch amplitudes, and at $St_h \approx 0.15-0.3$.
2. "Burst Mode" : C_t is very large, and propulsive (Froude) efficiencies are relatively low. The non-dimensional heave amplitude and St_h should be large.

Conclusion

The force measurements around the heaving and pitching hydrofoil indicate that the foil can generate large thrust coefficients, in excess of $C_t > 10$. These large thrust coefficients occur when the foil heave amplitude is very large, where strong leading edge vortices are observed. In all other flow cases, where the heave amplitude is not very large, the thrust coefficients are moderate, and the leading edge vortices on the foil are either small or non-existent. We provide evidence that the generation of large thrust coefficients by the foil is inextricably linked to the generation of a strong leading edge vortex on the foil, confirming the proposition made in [1].

References

[1] Anderson, J. M., Streitlien, K., Barrett, D. S. and Triantafyllou, M. S., Oscillating foils of high propulsive efficiency, *Journal of Fluid Mechanics*, **360**, 1998, 41–72.

[2] Fish, F. E. and Lauder, G. V., Passive and active flow control by swimming fishes and mammals, *Annual review of fluid mechanics*, **38**, 2006, 193 – 224.

[3] Hover, F. S., Haugsdal, O. and Triantafyllou, M. S., Effect of angle of attack profiles in flapping foil propulsion, *Journal of Fluids and Structures*, **19**, 2004, 37 – 47.

[4] Lau, T. C. W., Kelso, R. M. and Hassan, E. R., Flow visualisation of a pitching and heaving hydrofoil, in *Proceedings of the Fifteenth Australasian Fluid Mechanics Conference*, editors M. Behnia, W. Lin and G. D. McBain, University of Sydney, 2004.

[5] Read, D. A., Hover, F. S. and Triantafyllou, M. S., Forces on oscillating foils for propulsion and maneuvering, *Journal of Fluids and Structures*, **17**, 2003, 163 – 183.

[6] Rohr, J. J. and Fish, F. E., Strouhal number and optimization of swimming by odontocete cetaceans, *Journal of Experimental Biology*, **207**, 2004, 1633 – 1642.

[7] Sfakiotakis, M., Lane, D. M. and Davies, J. B. C., Review of fish swimming modes for aquatic locomotion, *IEEE Journal of Oceanic Engineering*, **24**, 1999, 237–252.

[8] Triantafyllou, G. S., Triantafyllou, M. S. and Grosenbaugh, M. A., Optimal thrust development in oscillating foils with application to fish propulsion, *Journal of Fluids and Structures*, **7**, 1993, 205–224.

[9] Triantafyllou, M. S., Triantafyllou, G. S. and Yue, D. K. P., Hydrodynamics of fishlike swimming, *Annual Review of Fluid Mechanics*, **32**, 2000, 33 – 53.

[10] Westerweel, J. and Scarano, F., Universal outlier detection for PIV data, *Experiments in Fluids*, **39**, 2005, 1096 – 1100.

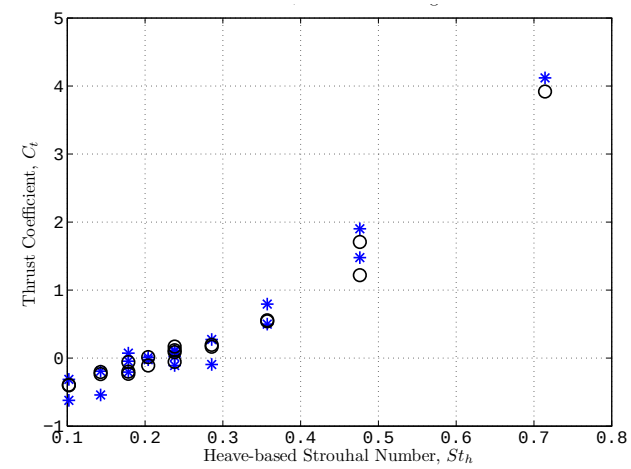

(a) Group I

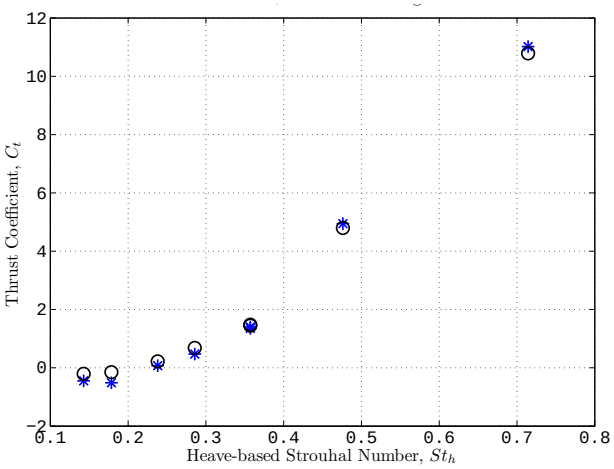

(b) Group II

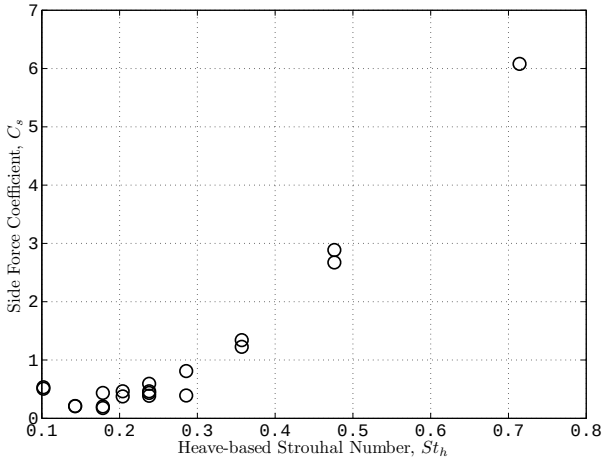

(c) Group I

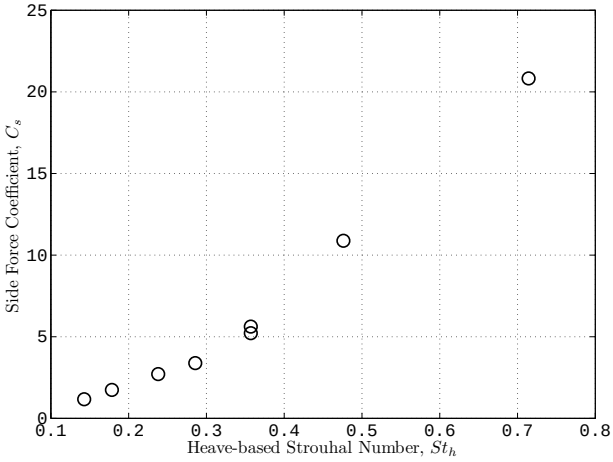

(d) Group II

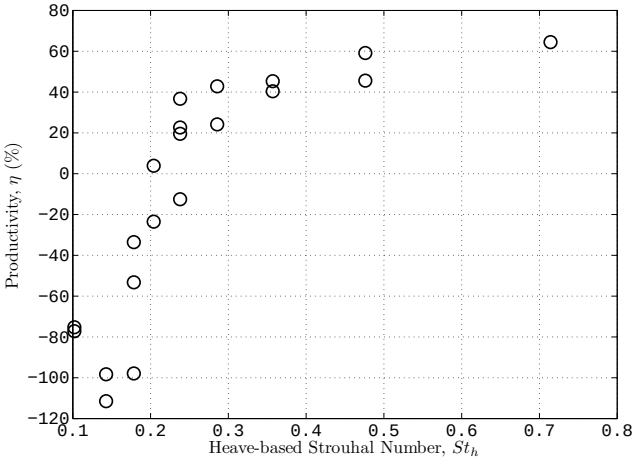

(e) Group I

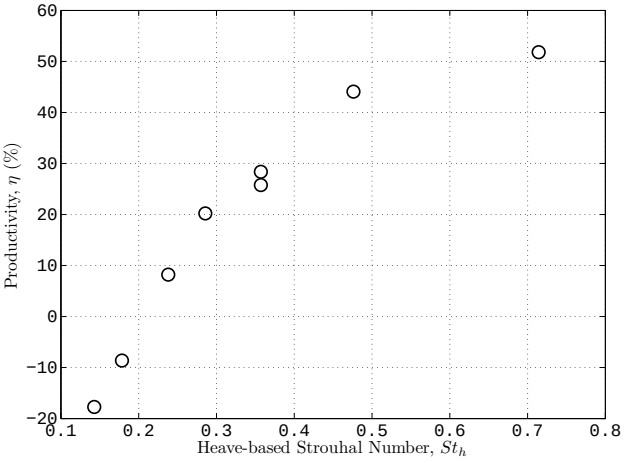

(f) Group II

Figure 2: Thrust and side force coefficients, C_t and C_s, and productivities η (%) for the unsteady foil for a,c,e) group I, $\frac{h_0}{c} = 0.5$, $\theta_0 = 30^o$ and b,d,f) group II, $\frac{h_0}{c} = 0.5$, $\theta_0 = 0^o$